Decadal predictability of tropical Indo-Pacific Ocean temperature trends due to anthropogenic forcing in a coupled climate model

Amy Solomon[1,2] and Matthew Newman[1,2]

Received 25 October 2010; revised 3 December 2010; accepted 22 December 2010; published 21 January 2011.

[1] This study quantifies the impact of ENSO on the decadal predictability of tropical Indo-Pacific Ocean trends in a very large ensemble of NCAR CCSM3 anthropogenically-forced (A1B scenario) simulations, by decomposing upper ocean temperatures into "ENSO" and "non-ENSO" variability. On decadal time scales, the ENSO pattern primarily contributes to the ensemble spread and has a trend whose amplitude is not predictable. However, the non-ENSO component of the trend has much smaller spread and is predictable after 10 years, much sooner than the total trend, which is predictable after 25 years. The non-ENSO component of the trend explains 96% of the total trend and has a structure that is distinct from ENSO, including cooling in the South Pacific due to increased southeast trades, warming of the warm pool, and strengthening of the equatorial Pacific near-surface temperature gradient superimposed upon a uniform warming.

Citation: Solomon, A., and M. Newman (2011), Decadal predictability of tropical Indo-Pacific Ocean temperature trends due to anthropogenic forcing in a coupled climate model, *Geophys. Res. Lett.*, *38*, L02703, doi:10.1029/2010GL045978.

1. Motivation

[2] For decadal climate forecasts to be useful they must provide verifiable regional skill on 10–30 year time scales. Much or even most of this skill may come from the forced response of the climate system to steadily increasing greenhouse gases (GhGs), a response that on multi-decadal-to-centennial time scales is potentially predictable compared to other sources of variability. However, predictability may be limited on shorter decadal time scales where the forced response and natural variability are of the same order of magnitude and share important regional details [see *Solomon et al.*, 2010]. For example, in many coupled climate models, the long-term response of the Indo-Pacific to an increase in GhGs shows some similarities to the pattern of variability observed during an El Niño/Southern Oscillation (ENSO) event, specifically increased sea surface temperatures (SSTs) in the equatorial central and eastern Pacific [see *Collins et al.*, 2005; *Liu et al.*, 2005; *DiNezio et al.*, 2010], causing the Intergovernmental Panel on Climate Change (IPCC) Fourth Assessment to refer to an "El Niño-like" trend [*Meehl et al.*, 2007].

[3] This issue is evident in the 50-year trend of wintertime tropical Indo-Pacific ocean temperatures averaged across a 40-member ensemble of Community Climate System Model Version 3 (CCSM3) simulations forced with GhGs following the IPCC Special Report on Emissions Scenarios (SRES) [*Nakicenovic et al.*, 2000] A1B scenario for the years 2010–2060 (Figures 1a–1c). Note that the domain average warming trend of 0.016 K/yr has been removed to highlight regional differences. The ensemble mean temperature trend pattern, **T**, has three-dimensional structure similar to the model's El Niño [see *Deser et al.*, 2006]. For example, the surface equatorial warming trend is flanked both north and south by subsurface cooling trends at 100–150 m depth (i.e., an anomalous steepening of the off-equatorial thermocline at ~10°N/S) in a pattern also typically observed during an El Niño event. On the other hand, in contrast to El Niño, equatorial warming occurs throughout the upper ocean with maximum warming of greater than 0.25 °C/decade east of 150°E and down to 100 meters, similar to the multi-model mean response to a doubling of CO_2 shown by *DiNezio et al.* [2009], and there is a notable north-south asymmetry throughout the upper 300 meters. **T** also explains more than 90% of the variance of ensemble mean wintertime ocean temperatures. Projecting the temperature field of each *i*th ensemble member θ_i onto **T** yields associated projection coefficient time series $\alpha_i(t)$ (see Figure 1d). The increase in the ensemble mean of $\alpha_i(t)$ is smaller than its ensemble spread for intervals up to 30 years, indicating that decadal forecasts of this trend pattern will have limited predictability.

[4] In this paper we hypothesize that ENSO variability is the primary contributor to the uncertainty of the trend on decadal time scales. If this is true, then removing the ENSO contribution to the trend will both enhance the predictability of the residual trend component and yield insight into those physical processes that drive the resulting more predictable pattern.

2. Separating Model Trends Into "ENSO" and "Non-ENSO" Components

[5] This study uses the National Center for Atmospheric Research Large Ensemble, two sets of 60-year CCSM3 integrations with identical initial conditions but different specified levels of GhGs [*Meehl et al.*, 2006]. The first set, the "commitment" or control simulations, has GhGs levels fixed at year 2000 levels and has 28 ensemble members, while the second set, the "A1B" or forced simulations, uses linearly increasing levels of GhGs following the SRES A1B scenario and has 40 ensemble members. The initial conditions for these runs are taken from a CCSM3 20th century historical (20C3M) simulation. The initial ocean fields are identical for all runs, while the initial atmospheric fields are taken from model output ±20 days from the ocean start date, January 1, 2000. The analysis uses wintertime (DJF) seasonal-mean ocean temperatures between 30°S to 30°N and 30°E to 70°W,

[1]PSD, ESRL, NOAA, Boulder, Colorado, USA.
[2]CDC, CIRES, University of Colorado at Boulder, Boulder, Colorado, USA.

Copyright 2011 by the American Geophysical Union.
0094-8276/11/2010GL045978

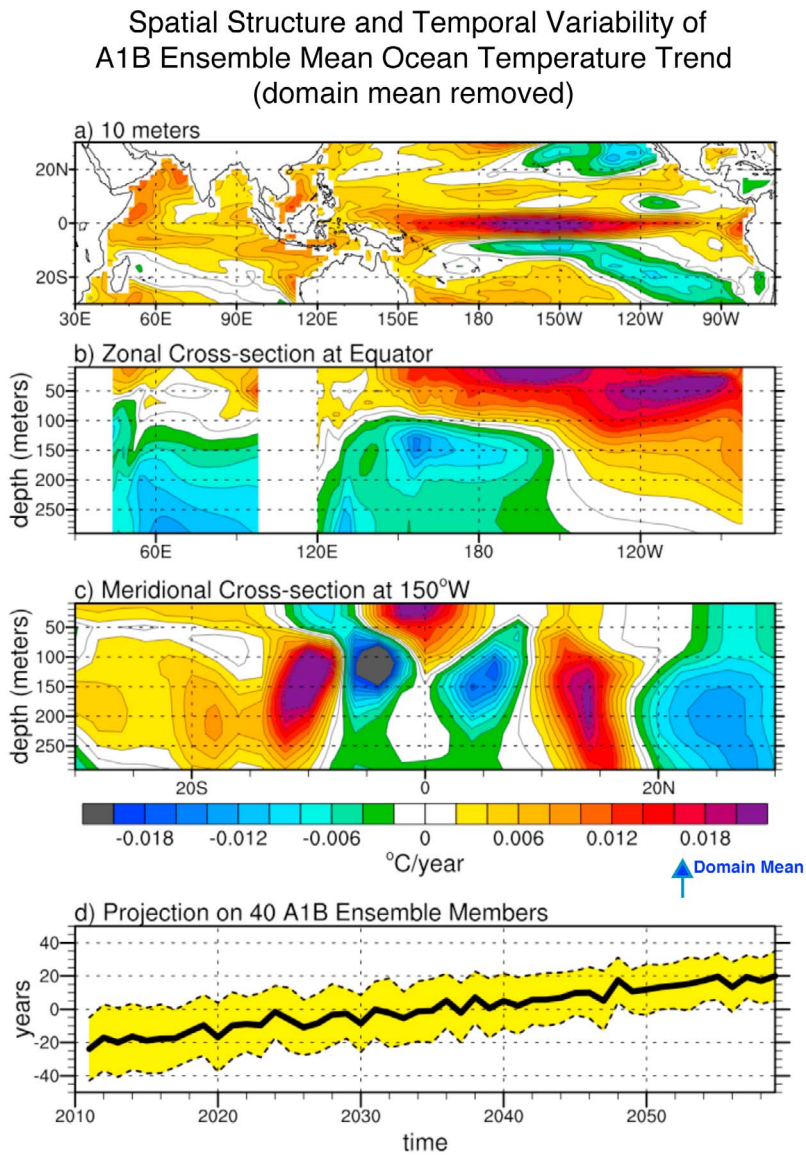

Figure 1. The total trend pattern of ensemble mean DJF ocean temperature in the A1B runs, in units of °C/year: (a) 10 meter temperatures; (b) longitude/depth cross-section along the equator (min/max = −0.014/0.025); (c) latitude/depth cross-section through 150°W (min/max = −0.037/0.031); (d) Projection of trend pattern on individual ensemble members, ensemble mean (solid) ± one standard deviation (dash), in units of years. This trend pattern explains 20.2% of the total DJF A1B variance and 90.3% of the DJF A1B ensemble mean variance. The domain mean (equal to 0.016 °C/year) has been removed to highlight spatial structure.

interpolated to depths from 10 meters to 290 meters at intervals of 20 meters.

[6] Many studies have attempted to separate observed variability into ENSO and non-ENSO components, but how to define ENSO structure can be problematic (see, for example, the different approaches of *Thompson et al.* [2009] and *Compo and Sardeshmukh* [2010] and also references therein). Beyond this, the observational record may be too short or the number of ensemble members too small to distinguish the trend pattern from natural ENSO variability. Additionally, the physical processes driving both ENSO and the ocean response to increased GhG forcing are not independent. Moreover, while most previous analyses based on observations have defined ENSO using SST alone, both ENSO variability and the response to external forcing have important subsurface details that require consideration.

[7] To overcome difficulties of identifying patterns of natural variability from forced integrations, we define a "natural" ENSO as the dominant three-dimensional empirical orthogonal function (3DEOF), $\mathbf{E}_1$, from the last 50 years of the control ensemble, shown in Figure 2. $\mathbf{E}_1$, explaining about one third of the total wintertime variance in the control runs, is the wintertime mature phase of ENSO in the CCSM3, known to be more meridionally confined and to extend too far into the western Pacific compared to observations. Still, the meridional structure of the subsurface temperature anomalies (Figure 2c) is consistent with poleward transport of heat off the equator at the peak of El Niño, and the slackening of the

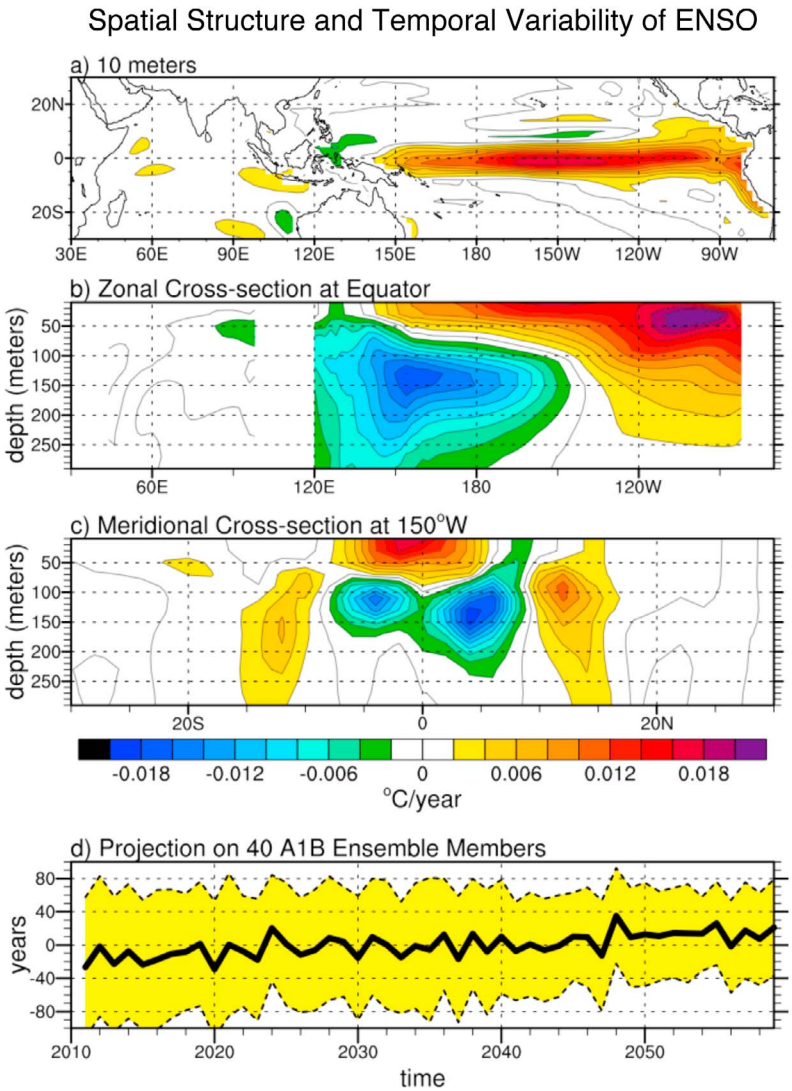

Figure 2. The dominant pattern of DJF ocean temperature variability in the commitment runs, scaled to indicate this pattern's contribution to the A1B ensemble mean trend, in units of °C/year: (a) 10 meter temperatures; (b) longitude/depth cross-section along the equator; (c) latitude/depth cross-section through 150°W; (d) Projection of the trend pattern on the 40 A1B individual ensemble members, ensemble mean (solid) ± one standard deviation (dash), in units of years. This pattern explains 32.2% variance in the commitment runs and 24.3% variance in the A1B runs. Note the y-axis in Figure 2d has twice the scale of Figures 1d and 3d.

thermocline along the equator (Figure 2b) resembles observed El Niño characteristics (see *Deser et al.* [2006] for a detailed description of ENSO in the CCSM3). Analysis of the higher order control 3DEOFs (not shown) finds that $\mathbf{E}_3$, explaining ~6% of the wintertime variance, may together with $\mathbf{E}_1$ comprise an ENSO dynamical structure: its pattern is reminiscent of an ENSO precursor and PC3 is significantly correlated (r = 0.35) at one-year lead with PC1. Including it as part of the ENSO definition has minimal impact on the results presented below, so for simplicity it has been excluded.

[8] We next define the ENSO component within the A1B simulations by projecting the temperature field of each ith ensemble member θ_i onto $\mathbf{E}_1$, yielding associated projection coefficient time series $\beta_i(t)$. Figure 2d shows the ensemble mean of $\beta_i(t)$ and its corresponding ensemble spread. This assumes ENSO has fixed spatial structure that, to first order, is unchanged as the climate evolves over a 60-year period, which is the case in our A1B ensemble (results not shown).

[9] Finally, we construct the "non-ENSO" component of the A1B ensemble by subtracting the ENSO component $\beta_i(t)$ $\mathbf{E}_1$ from each A1B ensemble member. The trend pattern $\mathbf{R}$ of the resulting residual non-ENSO dataset is then calculated in the same manner used for Figure 1. Results are shown in Figure 3 with the domain mean again removed. Strikingly, the ensemble spread of the corresponding projection coefficient time series $\gamma_i(t)$ is greatly reduced even as the ensemble mean captures most of the amplitude (Figure 3d).

[10] While the ENSO component is responsible for only ~5% of the ensemble mean trend within the entire ocean domain, it is primarily responsible for the equatorial near-surface warming in the central Pacific. Note that while the ENSO trend is significantly different from zero at the 99.99%

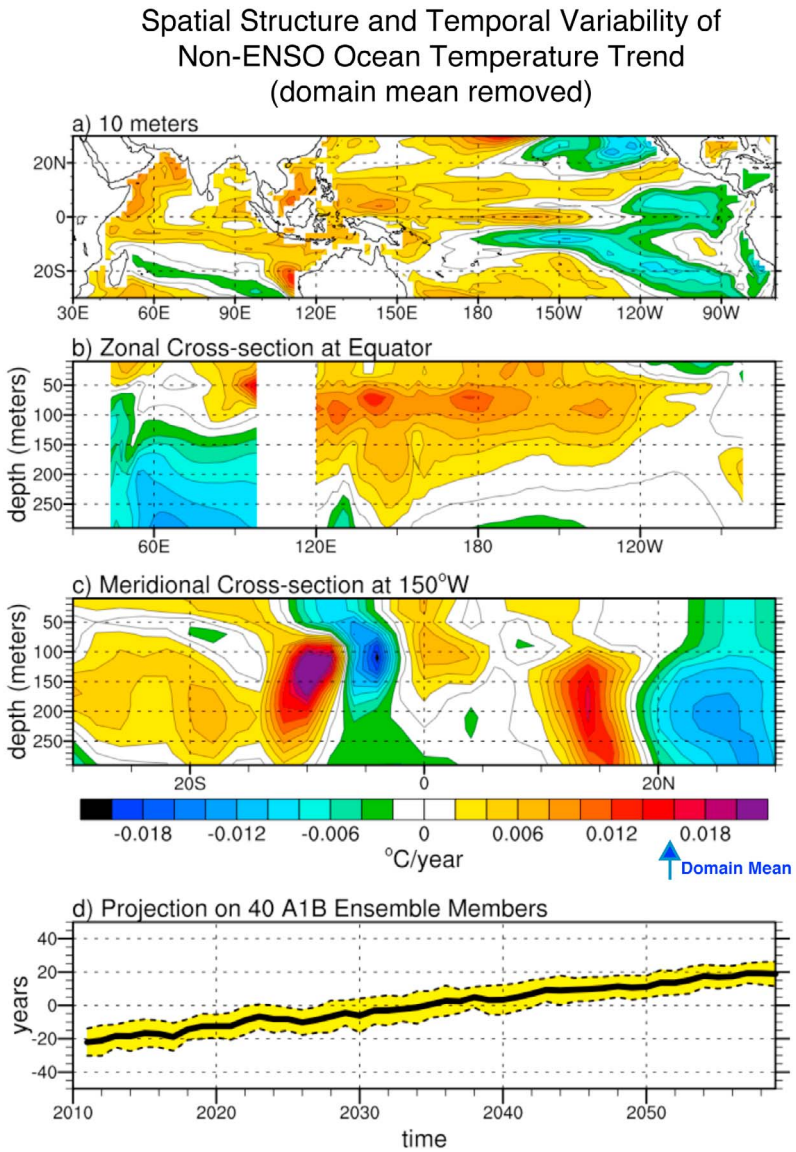

Figure 3. Non-ENSO ocean temperature trend pattern, in units of °C/year: (a) 10 meter temperatures; (b) longitude/depth cross-section along the equator; (c) latitude/depth cross-section through 150°W (min/max = −0.021/0.28); (d) Projection on individual ensemble members, ensemble mean (solid) ± one standard deviation (dash), in units of years. This pattern explains 16.5% of the total DJF A1B variance and 85.6% of the DJF A1B ensemble mean variance. The domain mean (equal to 0.016 °C/year) has been removed to highlight spatial structure.

level, the ensemble spread is so large that significant uncertainty in the *amplitude* of the ENSO trend remains over the entire run. The small reduction in the ensemble spread over the length of the run is statistically significant but does not affect our conclusions.

[11] Along the equator (Figure 3b), the non-ENSO trend has warming at all depths in the Pacific, with a maximum in the warm pool region between the surface and the thermocline. The stronger warming in the west acts to increase the climatological equatorial temperature gradient. The zonal structure of the equatorial Pacific warming is potentially driven by several processes with compensating effects, including a cooling due to an increase in near-surface vertical thermal stratification that enhances upwelling in the eastern equatorial Pacific [e.g., *Clement et al.*, 1996; *Cane et al.*, 1997], an increase in cloud cover in the western equatorial Pacific [see *DiNezio et al.*, 2009], and a warming due to enhanced downward longwave radiation associated with water vapor and lapse rate feedbacks [e.g., *Knutson and Manabe*, 1995]. Also, the subtropical warming is less than the tropical warming [see *Liu et al.*, 2005], which can cause relatively cooler water to subduct in the subtropics and upwell in the eastern equatorial Pacific, offsetting some externally-forced surface warming there [e.g., *Seager and Murtugudde*, 1997]. The most prominent subsurface feature, the dipole centered at 150°W in the South Pacific (Figure 3c), is consistent with strengthened southeast trades, as is the pronounced north-south asymmetry in the tropical Pacific [see *Xie et al.*, 2010].

[12] Removing the constraints imposed on the structure of ENSO with the 3DEOFs (specifically near-equatorial anomalies that maximize in the subsurface) by using only

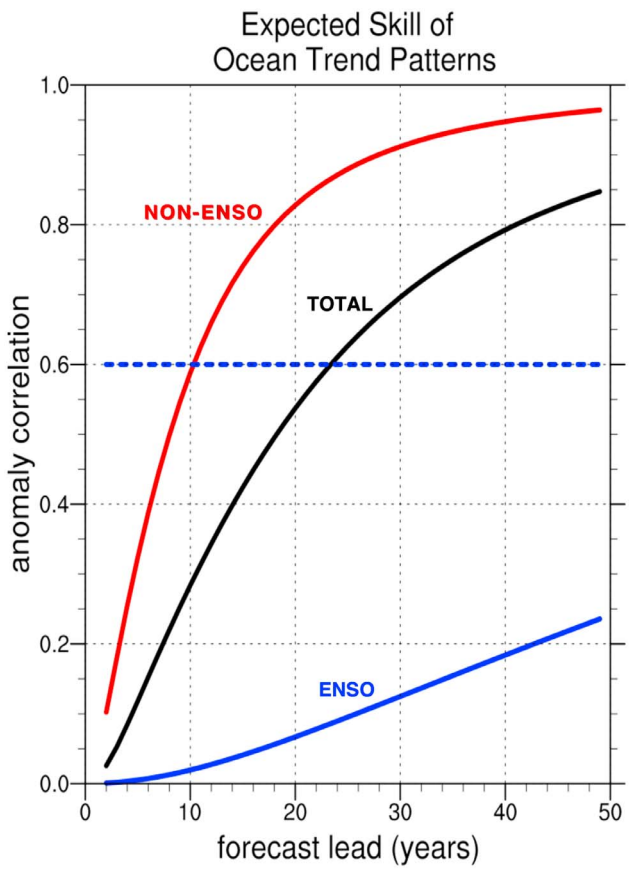

Figure 4. Expected skill of ensemble mean ocean temperature trend patterns for total A1B, non-ENSO, and ENSO fields (black, red, and blue lines, respectively). Anomaly correlations greater than 0.6 (dashed blue line) indicate an accepted level of useful skill. Under this criterion, the non-ENSO trend pattern is predictable after 10 years while the total trend pattern is predictable after 23 years. The ENSO trend pattern is not predictable in the last 50-year of the simulations.

10 meter data results in an ENSO component that explains a much greater fraction of the 10 meter A1B ensemble mean variance (28.1% vs. 3.6%) and a non-ENSO trend with an increased cooling in the central-to-eastern Pacific due to the projection of the 10 meter EOF on the trend (see Figure S1 of Text S1 of the auxiliary material).[1]

3. Predictability of trend components

[13] Perhaps the most striking feature of this decomposition is that the ensemble spread of the non-ENSO component is greatly reduced compared to that of the total trend pattern, even as the overall amplitude of the ensemble mean is about the same (cf. Figures 1d and 3d). This immediately suggests that within the context of this model the non-ENSO trend is considerably more robust than the overall trend and forecasts of it would be more skillful. To illustrate this point, we determine the predictability of each trend pattern, where predictability is defined in the usual way from expected "perfect-model" ensemble forecast skill, or how well the model forecasts itself given initial state uncertainty. When defined as the average anomaly correlation $\rho(\tau)$ between verification and ensemble mean forecast amplitudes at forecast lead τ, perfect-model forecast skill is also a simple function of the forecast signal-to-noise ratio S [*Sardeshmukh et al.*, 2000; *Newman et al.*, 2003]:

$$\rho(\tau) = \frac{S(\tau)}{[1 + S^2(\tau)]^{1/2}}$$

We determine S as the ratio of the signal $s(\tau) = s_o\,\tau$, where s_o is the (assumed constant, based on a least-squares fit) tendency of the ensemble mean trend time series for each component α, β, γ (Figures 1d, 2d, and 3d), to the noise σ, the corresponding root mean square ensemble spread assumed independent of τ. The resulting curves (Figure 4) show that the non-ENSO trend is generally much more predictable than the total trend. A corresponding result can be seen in the distinctive regional variation throughout the Indo-Pacific of $\rho(\tau = 10$, 20, and 30 yrs) determined from the local signal-to-noise ratio for the total trend at 10m depth (see Figure S2). For example, under a common operational criterion of minimum "useful" skill, $\rho = 0.6$, the amplitude of the non-ENSO trend is predictable after only 10 years whereas the amplitude of the total trend is not predictable for over 20 years. Interestingly, the ENSO-component of the trend is not predictable by this measure throughout the model run.

4. Summary and Discussion

[14] In this study we have decomposed the total projected anthropogenically-forced (A1B scenario) tropical Indo-Pacific ocean temperature trend into two components termed "ENSO" and "non-ENSO". We find the non-ENSO component to be much more robust across a large model ensemble than both the ENSO component and the total trend pattern, and correspondingly more predictable on decadal time scales. While the total trend has "El Niño-like" characteristics, in that the warming is greatest in the central equatorial Pacific and is similar to three-dimensional structures associated with ENSO, the predictable non-ENSO component of the trend has a structure distinct from ENSO with cooling in the South Pacific due to increased southeast trades, warming of the warm pool, and strengthening of the equatorial Pacific near-surface temperature gradient superimposed upon uniform warming. The robustness of this structure across ensemble members suggests a physically meaningful response to external forcing. Also, the relatively small ensemble mean amplitude of the ENSO component compared to its spread suggests that quantitatively determining SST trends induced by both future anthropogenic forcing (in coupled GCMs) and past external forcing (in observations) may require much larger ensembles and longer datasets than have generally been used in past studies.

[15] This decomposition might have yielded a trivial result if the non-ENSO component had a similar ensemble spread to the total trend, or if the non-ENSO component had explained a small part of the total trend, or if removing an El Niño-like trend component had left a La Niña-like residual trend. However, none of these possibilities were realized.

[16] While this striking result was obtained using a fairly simple statistical approach to isolate ENSO variability in this

[1]Auxiliary materials are available in the HTML. doi:10.1029/2010GL045978.

model, the nature of ENSO in other coupled climate models might require more complex approaches. In addition, treating ENSO and non-ENSO components as independent could be an oversimplification for those models in which they more strongly interact. On the other hand, this model underestimates natural ENSO decadal variance [*Newman*, 2007] so it might overestimate externally-forced ENSO trend predictability.

[17] It bears repeating that this study does not show that the pattern in Figure 3 is the "true" trend. Rather, Figure 3 represents the component of the trend that is predictable on decadal time scales. Consequently, beyond the practical limitations of small ensembles and imperfect models, real-world decadal forecast skill will be limited by the substantial contribution to the total realized trend of unpredictable ENSO events that occur during the forecast period. To properly evaluate the upcoming AR5 decadal experiments it will be necessary to determine how ENSO degrades the skill of the trend forecasts. The strategy employed here to assess predictability could also be used to identify a priori where skill lies in decadal forecasts of the tropical ocean and its associated global teleconnections.

[18] **Acknowledgments.** The authors thank the NCAR CCR section for executing the simulations and two anonymous reviewers, M. Alexander, G. Compo, C. Deser, P. Gent, J. Perlwitz, and P. Sardeshmukh for helpful comments. This work was supported by grants from NOAA OAR CVP Program.

References

Cane, M. A., A. C. Clement, A. Kaplan, Y. Kushnir, D. Pozdnyakov, R. Seager, S. E. Zebiak, and R. Murtugudde (1997), Twentieth century sea surface temperature trends, *Science*, *275*, 957–960, doi:10.1126/science.275.5302.957.

Clement, A. C., R. Seager, M. A. Cane, and S. E. Zebiak (1996), An ocean dynamical thermostat, *J. Clim.*, *9*, 2190–2196, doi:10.1175/1520-0442(1996)009<2190:AODT>2.0.CO;2.

Collins, M., et al. (2005), El Niño- or La Niña-like climate change?, *Clim. Dyn.*, *24*, 89–104, doi:10.1007/s00382-004-0478-x.

Compo, G. P., and P. D. Sardeshmukh (2010), Removing ENSO-related variations from the climate record, *J. Clim.*, *23*, 1957–1978, doi:10.1175/2009JCLI2735.1.

Deser, C., A. Capotondi, R. Saravanan, and A. S. Phillips (2006), Tropical Pacific and Atlantic climate variability in CCSM3, *J. Clim.*, *19*, 2451–2481, doi:10.1175/JCLI3759.1.

DiNezio, P., A. Clement, G. A. Vecchi, B. J. Soden, B. Kirtman, and S.-K. Lee (2009), Climate response of the equatorial Pacific to global warming, *J. Clim.*, *22*, 4873–4892, doi:10.1175/2009JCLI2982.1.

DiNezio, P., A. Clement, and G. A. Vecchi (2010), Reconciling differing views of tropical Pacific climate change, *Eos Trans. AGU*, *91*(16), 141, doi:10.1029/2010EO160001.

Knutson, T. R., and S. Manabe (1995), Time- mean response over the tropical Pacific to increased CO_2 in a coupled ocean- atmosphere model, *J. Clim.*, *8*, 2181–2199, doi:10.1175/1520-0442(1995)008<2181:TMROTT>2.0.CO;2.

Liu, Z., S. Vavrus, F. He, N. Wen, and Y. Zhong (2005), Rethinking tropical ocean response to global warming: The enhanced equatorial warming, *J. Clim.*, *18*, 4684–4700, doi:10.1175/JCLI3579.1.

Meehl, G. A., W. M. Washington, B. D. Santer, W. D. Collins, J. M. Arblaster, A. Hu, D. M. Lawrence, H. Teng, L. E. Buja, and W. G. Strand Jr. (2006), Climate change projections for the 21st century and climate change commitment in the CCSM3, *J. Clim.*, *19*, 2597–2616, doi:10.1175/JCLI3746.1.

Meehl, G. A., et al. (2007), Global climate projections, in *Climate Change 2007: The Physical Science Basis: Contribution of Working Group I to the Fourth Assessment Report of the Intergovernmental Panel on Climate Change*, edited by S. Solomon et al., pp. 747–845, Cambridge Univ. Press, New York.

Nakicenovic, N., et al. (2000), *Intergovernmental Panel on Climate Change Special Report on Emissions Scenarios*, Cambridge Univ. Press, New York.

Newman, M. (2007), Interannual to decadal predictability of tropical and North Pacific sea surface temperatures, *J. Clim.*, *20*, 2333–2356, doi:10.1175/JCLI4165.1.

Newman, M., P. D. Sardeshmukh, C. R. Winkler, and J. S. Whitaker (2003), A study of subseasonal predictability, *Mon. Weather Rev.*, *131*, 1715–1732, doi:10.1175//2558.1.

Sardeshmukh, P. D., G. P. Compo, and C. Penland (2000), Changes in probability associated with El Niño, *J. Clim.*, *13*, 4268–4286, doi:10.1175/1520-0442(2000)013<4268:COPAWE>2.0.CO;2.

Seager, R., and R. Murtugudde (1997), Ocean dynamics, thermocline adjustment and regulation of tropical SST, *J. Clim.*, *10*, 521–534, doi:10.1175/1520-0442(1997)010<0521:ODTAAR>2.0.CO;2.

Solomon, A., et al. (2010), Distinguishing the roles of natural and anthropogenically forced decadal climate variability: Implications for prediction, *Bull. Am. Meteorol.. Soc.*, doi:10.1175/2010BAMS2962.1, in press.

Thompson, D. W. J., J. M. Wallace, P. D. Jones, and J. Kennedy (2009), Identifying signatures of natural climate variability in time series of global-mean surface temperature: Methodology and Insights, *J. Clim.*, *22*, 6120–6141, doi:10.1175/2009JCLI3089.1.

Xie, S.-P., C. Deser, G. A. Vecchi, J. Ma, H. Teng, and A. T. Wittenberg (2010), Global warming pattern formation: Sea surface temperature and rainfall, *J. Clim.*, *23*, 966–986, doi:10.1175/2009JCLI3329.1.

M. Newman and A. Solomon, CDC, CIRES, University of Colorado at Boulder, Boulder, CO 80305, USA.